Long-lasting fibrin matrices ensure stable and functional angiogenesis by highly tunable, sustained delivery of recombinant VEGF$_{164}$

Veronica Sacchi[a], Rainer Mittermayr[b], Joachim Hartinger[b], Mikaël M. Martino[c], Kristen M. Lorentz[c], Susanne Wolbank[b], Anna Hofmann[b], Remo A. Largo[d], Jeffrey S. Marschall[e,f], Elena Groppa[a], Roberto Gianni-Barrera[a], Martin Ehrbar[e], Jeffrey A. Hubbell[c], Heinz Redl[b], and Andrea Banfi[a,1]

[a]Cell and Gene Therapy, Department of Biomedicine, University of Basel, and Department of Surgery, Basel University Hospital, CH-4031 Basel, Switzerland; [b]Ludwig Boltzmann Institute for Experimental and Clinical Traumatology, Austrian Cluster for Tissue Regeneration, Allgemeine Unfallversicherungsanstalt, A-1200 Vienna, Austria; [c]Institute of Bioengineering, School of Life Sciences and School of Engineering, Ecole Polytechnique Fédérale de Lausanne, CH-1015 Lausanne, Switzerland; Departments of [d]Urology and [e]Obstetrics, Zurich University Hospital, CH-8091 Zurich, Switzerland; and [f]University of Louisville School of Dentistry, Louisville, KY 40202

Edited by Robert Langer, Massachusetts Institute of Technology, Cambridge, MA, and approved April 3, 2014 (received for review March 13, 2014)

Clinical trials of therapeutic angiogenesis by vascular endothelial growth factor (VEGF) gene delivery failed to show efficacy. Major challenges include the need to precisely control in vivo distribution of growth factor dose and duration of expression. Recombinant VEGF protein delivery could overcome these issues, but rapid in vivo clearance prevents the stabilization of induced angiogenesis. Here, we developed an optimized fibrin platform for controlled delivery of recombinant VEGF, to robustly induce normal, stable, and functional angiogenesis. Murine VEGF$_{164}$ was fused to a sequence derived from α2-plasmin inhibitor (α_2-PI$_{1-8}$) that is a substrate for the coagulation factor fXIIIa, to allow its covalent cross-linking into fibrin hydrogels and release only by enzymatic cleavage. An α_2-PI$_{1-8}$–fused variant of the fibrinolysis inhibitor aprotinin was used to control the hydrogel degradation rate, which determines both the duration and effective dose of factor release. An optimized aprotinin-α_2-PI$_{1-8}$ concentration ensured ideal degradation over 4 wk. Under these conditions, fibrin-α_2-PI$_{1-8}$-VEGF$_{164}$ allowed exquisitely dose-dependent angiogenesis: concentrations ≥25 μg/mL caused widespread aberrant vascular structures, but a 500-fold concentration range (0.01–5.0 μg/mL) induced exclusively normal, mature, nonleaky, and perfused capillaries, which were stable after 3 mo. Optimized delivery of fibrin-α_2-PI$_{1-8}$-VEGF$_{164}$ was therapeutically effective both in ischemic hind limb and wound-healing models, significantly improving angiogenesis, tissue perfusion, and healing rate. In conclusion, this optimized platform ensured (*i*) controlled and highly tunable delivery of VEGF protein in ischemic tissue and (*ii*) stable and functional angiogenesis without introducing genetic material and with a limited and controllable duration of treatment. These findings suggest a strategy to improve safety and efficacy of therapeutic angiogenesis.

Therapeutic angiogenesis is an attractive strategy for treating ischemic conditions, such as peripheral and coronary artery diseases or chronic wounds, in which the intrinsic capacity for spontaneous vascular repair and tissue regeneration is either compromised or insufficient to restore physiological blood flow. In fact, sufficient expansion of microvascular networks is capable of increasing flow in upstream collateral arteries through retrograde signals (1, 2), thereby providing effective bypass of the obstructed feeding vessels. Vascular endothelial growth factor (VEGF) is the master regulator of both developmental and reparative vascular growth (3). However, initial clinical trials of VEGF gene delivery failed to establish clinical benefit (4). Retrospective analyses identified several issues that undermined the efficacy of those trials, particularly the difficulty to deliver a sufficient VEGF dose into the target tissue at safe vector doses (5, 6). By cell-based gene delivery, we previously found that, to effectively exploit VEGF's therapeutic potential and robustly induce only functional and safe angiogenesis, it is key to control its microenvironmental concentration around each producing cell in vivo rather than its total dose (7) as VEGF binds tightly to the extracellular matrix (ECM) (8). However, it is challenging to achieve homogeneous expression levels in vivo with gene-therapy vectors. Further, newly induced vessels require sustained VEGF stimulation for at least 4 wk to stabilize and persist indefinitely, but unlimited duration of expression raises safety concerns (7, 9, 10). Controlled release of recombinant VEGF protein from biodegradable matrices is an attractive approach for clinical translation of these biological concepts due to the lack of genetic modification, the ease of achieving a homogenous dose distribution, and the limited duration of treatment (11).

Physiological angiogenesis crucially depends on a spatially restricted organization of growth factors through their binding to the ECM (12). Fibrin, a natural product of blood coagulation, provides unique features for physiological presentation of angiogenic signals: (*i*) It is injectable as a liquid and solidifies in situ without cytotoxicity; (*ii*) it is remodeled by cell-associated enzymes

Significance

Inducing the growth of new blood vessels by specific factors is an attractive strategy to restore blood flow in ischemic tissues. Vascular endothelial growth factor (VEGF) is the master regulator of angiogenesis, yet clinical trials of VEGF gene delivery failed. Major challenges include the need to control the tissue distribution of factor dose and the duration of expression. Here, we developed a highly tunable fibrin-based platform to precisely control the dose and duration of VEGF protein delivery in tissues. Optimized delivery of fibrin-bound VEGF ensured normal, stable, and functional angiogenesis and improved perfusion of ischemic tissues, without genetic modification and with limited duration of VEGF delivery. These findings suggest a strategy to improve both safety and efficacy of therapeutic angiogenesis.

Author contributions: V.S., R.M., M.E., J.A.H., H.R., and A.B. designed research; V.S., R.M., J.H., M.M.M., S.W., A.H., R.A.L., J.S.M., E.G., and R.G.-B. performed research; M.M.M., K.M.L., S.W., and A.H. contributed new reagents/analytic tools; V.S., R.M., M.M.M., S.W., A.H., J.S.M., E.G., and A.B. analyzed data; and V.S., R.M., M.E., J.A.H., H.R., and A.B. wrote the paper.

Conflict of interest statement: The fibrin gel immobilization scheme is the subject of patents upon which J.A.H. is named as inventor and has been licensed by a company in which J.A.H. is a shareholder.

This article is a PNAS Direct Submission.

[1]To whom correspondence should be addressed. E-mail: Andrea.Banfi@usb.ch.

This article contains supporting information online at www.pnas.org/lookup/suppl/doi:10.1073/pnas.1404605111/-/DCSupplemental.

like metalloproteinases and plasmin; and (*iii*) it is a natural cell-infiltration matrix (13). Therefore, we previously developed an approach to enzymatically link growth factors into fibrin hydrogels: the α_2-plasmin inhibitor-derived octapeptide NQEQVSPL (α_2-PI_{1-8}), which is a substrate for the transglutaminase coagulation factor fXIIIa and has no plasmin inhibitory function itself, fused onto a factor N terminus, ensures its covalent binding to fibrin during the fibrinogen cross-linking reaction and subsequent release only through matrix degradation by local cell-associated proteases (14, 15). Matrix-bound presentation of diverse so-engineered growth factors, such as α_2-PI_{1-8}–fused variants of VEGF-A_{121}, BMP-2, and IGF1, considerably accentuated their biological effects compared with the wild-type factors (16–19). However, the brief persistence of fibrin hydrogels in vivo (16) is insufficient to ensure stabilization of newly induced vessels and is a major obstacle to its exploitation for therapeutic angiogenesis (20). To gain control over fibrin-remodeling rates and significantly prolong gel persistence in vivo, we have engineered an α_2-PI_{1-8}–fused variant of the fibrinolysis inhibitor aprotinin (21). Here, we developed a fibrin platform to ensure both controlled and sustained delivery of α_2-PI_{1-8}-VEGF-A_{164} and achieve robust induction of normal, stable, and functional angiogenesis in therapeutically relevant target tissues.

Results

Generation of a Recombinant Murine $VEGF_{164}$ Variant, α_2PI_{1-8}-$VEGF_{164}$. The α_2-PI_{1-8} peptide was fused at the N terminus of murine $VEGF_{164}$ by a previously developed method of protein engineering (15). The coupling efficiency of α_2-PI_{1-8}-$VEGF_{164}$ in fibrin gels was determined measuring the factor release into buffer every 24 h over 7 d: 5.1 ± 1.2% of the incorporated α_2-PI_{1-8}-$VEGF_{164}$ was released in the first day without significant increases by 7 d (6.9 ± 1.2%) whereas the native $VEGF_{164}$ was almost completely released already after 1 d (88.2 ± 2.4%) (Fig. S1*A*). The bioactivity of α_2-PI_{1-8}-$VEGF_{164}$ was equivalent to native $VEGF_{164}$, as determined by their ability to induce VEGFR-2 phosphorylation on endothelial cells (Fig. S1*B*).

In Vivo Fibrin-Gel Degradation as a Function of Composition. Fibrinogen content proportionally determines the maximum amount of α_2-PI_{1-8}-VEGF incorporated into the gel. Therefore, the highest concentration compatible with in vivo injection in liquid form (polymerization time >10 s) was determined to be 25 mg/mL and selected for subsequent experiments. Small-strain oscillatory shear rheometry showed that gel stiffness varied between 2.9 ± 0.4 and 6.9 ± 1.2 kPa, depending on the concentration of cross-linking enzymes. To determine the effect of gel composition on in vivo degradation rate after intramuscular injection, the amount of remaining gel was assessed by histological analysis after 4 d (Fig. S2*A*) and by noninvasive multispectral imaging of gels labeled with fluorescent fibrinogen (Fig. S2*B*). All compositions showed similar gel persistence and degradation rates, being essentially consumed by 5 d (Fig. S2). Therefore, the composition with the lowest stiffness (2.9 kPa: fibrinogen 25 mg/mL, FXIII 2 U/mL, thrombin 2 U/mL) was selected to investigate growth-factor delivery in vivo, to maximize compliance and minimize tissue invasiveness.

Aprotinin-α_2-PI_{1-8} Concentration Determines both Rate and Duration of VEGF Release. Aprotinin inhibits fibrin degradation by proteases, and the engineered variant aprotinin-α_2-PI_{1-8} (21) was covalently cross-linked in the gels to prolong in vivo persistence and the duration of VEGF release, required for vascular stabilization. Gel degradation rate affects both key parameters controlling angiogenesis (i.e., the rate and duration of VEGF release), but in opposite directions, as a reduction in degradation rate would increase the duration of VEGF release but also reduce its rate (i.e., the effective delivered dose). Therefore, we first sought to determine the optimal aprotinin-α_2-PI_{1-8} concentration that would ensure both sufficient in vivo persistence and an adequate VEGF release rate. Gels were prepared with the maximum α_2-PI_{1-8}-$VEGF_{164}$ concentration that would not affect their mechanical properties (100 μg/mL) and a fourfold lower one (25 μg/mL), in combination with three different aprotinin-α_2-PI_{1-8} concentrations (17 μg/mL, 56 μg/mL, and 85 μg/mL), to analyze the effect of aprotinin-α_2-PI_{1-8} dose on the effective VEGF release rate, based on induced vascular morphology. As shown in Fig. 1, 9 d after intramuscular injection, the negative control gels, containing only aprotinin-α_2-PI_{1-8}, did not induce any angiogenesis whereas 100 μg/mL α_2-PI_{1-8}-$VEGF_{164}$ induced aberrant vessels independently of aprotinin concentration. Such vessels displayed irregularly dilated diameters and multiple lumens, were devoid of pericytes, and were covered with a thick layer of smooth muscle cells, similar to previously described angioma-like structures induced by excessive VEGF doses (7). However, the effects of the fourfold lower α_2-PI_{1-8}-$VEGF_{164}$ concentration of 25 μg/mL were clearly dependent on aprotinin-α_2-PI_{1-8} amount: no angiogenesis was detectable with 85 μg/mL, aberrant angioma-like structures were induced with 17 μg/mL, and an abundant network of morphologically normal, pericyte-covered capillaries was generated with the intermediate 56 μg/mL concentration, even if rare enlarged vessels were still detectable. Thus, an aprotinin-α_2-PI_{1-8} concentration of 56 μg/mL, which allowed a VEGF dose-dependent transition between normal and aberrant angiogenesis, was used in subsequent experiments.

α_2-PI_{1-8}-$VEGF_{164}$ Bioactivity After Gel Incorporation and in Vivo Implantation. To determine whether α_2-PI_{1-8}-$VEGF_{164}$ could retain its bioactivity while incorporated into the fibrin gels in vivo, before being released, gels were preformed at 37 °C with 100 μg/mL α_2-PI_{1-8}-$VEGF_{164}$ and 56 μg/mL aprotinin-α_2-PI_{1-8} and implanted s.c. in nude mice. After 2 wk, gels still contained

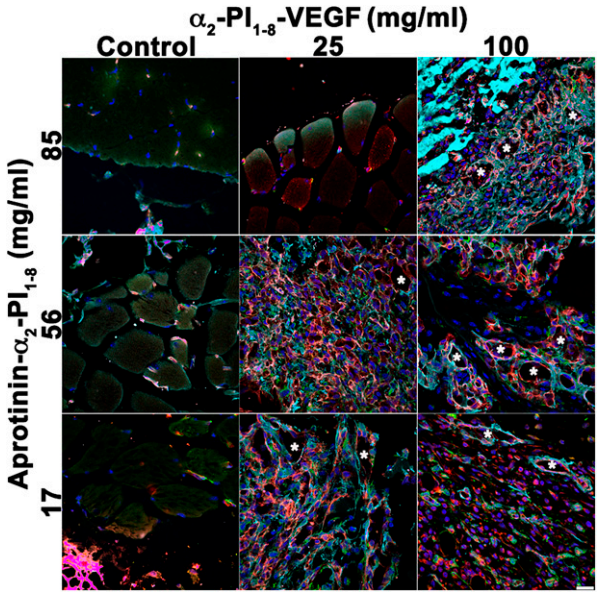

Fig. 1. Aprotinin-α_2-PI_{1-8} concentration determines the effective released dose of α_2-PI_{1-8}-$VEGF_{164}$ and the angiogenic outcome. Fibrin gels were injected into the gastrocnemius muscles of SCID mice, and tissues were analyzed 9 d later. Two different α_2-PI_{1-8}-$VEGF_{164}$ concentrations (25 μg/mL and 100 μg/mL) were tested in combination with three aprotinin-α_2-PI_{1-8} concentrations (17 μg/mL, 56 μg/mL, and 81 μg/mL). Negative control conditions contained only aprotinin-α_2-PI_{1-8}. Frozen sections were immunostained for endothelial cells (CD31, in red), pericytes (NG2, in green), smooth-muscle cells (α-SMA, in cyan) and nuclei (DAPI, in blue). Asterisks, enlarged aberrant vascular structures. $n = 3$. (Scale bar: 20 μm.)

~30% of the α_2-PI_{1-8}-$VEGF_{164}$ amount incorporated at day 0 (Fig. S3*A*). Furthermore, α_2-PI_{1-8}-$VEGF_{164}$ extracted from gels after 2 wk of in vivo incubation was capable of inducing endothelial proliferation as efficiently as the nonimplanted factor (Fig. S3*B*), indicating that gel incorporation effectively protects VEGF bioactivity despite prolonged in vivo exposure. The extracted factor showed a slightly reduced activity compared with fresh recombinant VEGF (~80% relative efficacy) as a consequence of the prolonged manipulations necessary for the gel-extraction procedure.

Dose-Dependent Angiogenesis by Fibrin-Bound α_2-PI_{1-8}-$VEGF_{164}$. Since decreasing α_2-PI_{1-8}-$VEGF_{164}$ from 100 μg/mL to 25 μg/mL caused a shift from completely aberrant to mostly normal angiogenesis, we investigated the effects of lower α_2-PI_{1-8}-$VEGF_{164}$ concentrations. Nine days after intramuscular injection, 5 μg/mL, 1 μg/mL, and 0.1 μg/mL α_2-PI_{1-8}-$VEGF_{164}$ all induced exclusively normal and mature capillaries, associated with nerve/glia antigen 2 (NG2)-positive and α-smooth muscle actin (α-SMA)-negative pericytes (Fig. S4).

Sustained VEGF stimulation for at least 4 wk is necessary for newly induced vessels to stabilize and become VEGF-independent (7, 9, 10). Four weeks after intramuscular implantation of gels carrying four different α_2-PI_{1-8}-$VEGF_{164}$ concentrations (0.01 μg/mL, 0.1 μg/mL, 5 μg/mL, and 100 μg/mL), small amounts of nondegraded gel were still detectable (Fig. S5), and robust angiogenesis was present in all conditions (Fig. 2 *A* and *D*). Similarly to the 9-d results, 100 μg/mL α_2-PI_{1-8}-$VEGF_{164}$ generated aberrant angioma-like structures mixed with more regular capillaries, which were, however, completely devoid of mural cells whereas both 0.1 μg/mL and 5 μg/mL induced exclusively normal networks of mature capillaries. Remarkably, the further 10-fold lower VEGF concentration of 0.01 μg/mL also induced efficient capillary growth, suggesting that normal angiogenesis can be effectively generated by a very wide range of α_2-PI_{1-8}-$VEGF_{164}$ doses. All vessels induced by α_2-PI_{1-8}-$VEGF_{164}$ concentrations up to 5 μg/mL displayed the morphology of normal skeletal-muscle capillaries as they were covered by $NG2^+/SMA^-$ pericytes, but no SMA^+ smooth muscle (22) and had homogeneous diameter distributions in a narrow range within 10 μm (90th percentile, 0.01 μg/mL = 4.62 μm; 0.1 μg/mL = 4.53 μm; 5 μg/mL = 8.47 μm), similar to normal capillaries in control tissues (90th percentile, 4.48 μm). In contrast, aberrant structures induced by 100 μg/mL displayed very heterogeneous and enlarged sizes (90th percentile, 16.05 μm) and were covered by a thick smooth-muscle coat (Fig. 2 *A* and *B*). Interestingly, concentrations ≤0.1 μg/mL induced vessels with the same average diameter as control tissue whereas the capillaries induced by 5 μg/mL were significantly larger (Fig. 2*C*), although homogeneous in size and smaller than 10 μm and normal in morphology. In contrast to vessel diameters, the amount of angiogenesis, quantified as vessel length density (VLD), did not depend on the α_2-PI_{1-8}-$VEGF_{164}$ dose as all concentrations between 0.01 μg/mL and 5 μg/mL similarly increased VLD by 50–60% compared with controls (Fig. 2*D*).

Sustained vascular leakage is a side effect of VEGF delivery that can lead to harmful tissue edema (23). Therefore, plasma leakage was quantified 4 wk after implantation of gels containing 5 μg/mL α_2-PI_{1-8}-$VEGF_{164}$: i.e., the highest concentration inducing morphologically normal angiogenesis at the latest time when gel-bound factor was still present (Fig. S5). Consistent with previous results (7), newly induced normal vessels were not leaky after 4 wk of VEGF delivery, with similar levels of Evans blue extravasation as the background measured in control tissues implanted with empty gels containing no VEGF (controls, 6.49 ± 1.54 ng Evans blue/mg tissue vs. VEGF, 5 μg/mL, 6.98 ± 1.83 ng Evans blue/mg tissue; P = n.s.), suggesting they had acquired normal functionality. Moreover, no macroscopic edema was observed in the implanted limbs at any time up to 3 mo.

Long-Term Stability and Perfusion of Vessels Induced by Optimized α_2-PI_{1-8}-$VEGF_{164}$ Delivery. We assessed whether α_2-PI_{1-8}-$VEGF_{164}$–induced vessels had stabilized and achieved complete independence from exogenous VEGF 3 mo after intramuscular gel injection. Angiogenesis was still present in all conditions, displaying similar morphologies as after 4 wk (Fig. 3*A*) although no trace of the injected gels could be found anymore (Fig. S5). All α_2-PI_{1-8}-$VEGF_{164}$ concentrations causing normal angiogenesis (0.01–5 μg/mL) induced about a 70% increase in VLD, which was also significantly more than the amount still present after delivery of 100 μg/mL that induced aberrant angiogenesis (Fig. 3*B*). A comparison between VLD after 3 mo and 4 wk showed that the normal vessels generated by concentrations between 0.01 μg/mL and 5 μg/mL were completely stable and even further increased whereas greater than 60% of the aberrant vasculature induced by 100 μg/mL regressed (Fig. 3*C*). Further, i.v. injection of a fluorescein-labeled tomato lectin (FITC-lectin) showed that essentially all endothelial structures induced by the different α_2-PI_{1-8}-$VEGF_{164}$ concentrations were reached by blood flow and thereby functionally connected to the systemic circulation both after 4 wk (Fig. S6) and 3 mo (Fig. S7), as demonstrated by colocalization of CD31 immunostaining and FITC-lectin. Therefore, optimized delivery of fibrin-bound α_2-PI_{1-8}-$VEGF_{164}$ induced the growth of morphologically normal and mature capillary networks that were both stable and functional.

Functional Improvement in Ischemia. Lastly, we tested the efficacy of optimized delivery of fibrin-bound α_2-PI_{1-8}-$VEGF_{164}$ to cause functional improvement in two different rodent models of clinically relevant ischemic diseases: i.e., hind-limb ischemia and ischemic wound healing.

Based on the results described in Figs. 2 and 3 for normal skeletal muscle, two α_2-PI_{1-8}-VEGF concentrations in a 10-fold range (0.5 μg/mL and 5 μg/mL) were delivered through the optimized gel composition in a murine model of hind-limb ischemia.

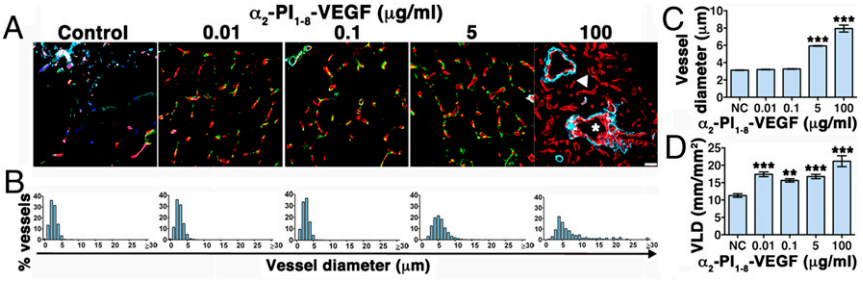

Fig. 2. Dose-dependent angiogenesis 4 wk after optimized delivery of fibrin-bound α_2-PI_{1-8}-$VEGF_{164}$. Fibrin gels containing 56 μg/mL aprotinin-α_2-PI_{1-8} and 0 μg/mL (negative control), 0.01 μg/mL, 0.1 μg/mL, 5 μg/mL, or 100 μg/mL α_2-PI_{1-8}-$VEGF_{164}$ were injected into gastrocnemius muscles of SCID mice. Tissues were analyzed 4 wk later. (*A*) Frozen sections were immunostained to detect endothelial cells (CD31, in red), pericytes (NG2, in green), and smooth-muscle cells (α-SMA, in cyan). n = 3. (Scale bar: 20 μm.) Asterisks, enlarged aberrant vascular structures; arrowhead, regular capillaries devoid of mural cells. (*B* and *C*) Quantification of vessel diameters (n > 500 per group), shown as their distribution in 1-μm intervals (*B*) and mean ± SEM (*C*). (*D*) The amount of angiogenesis was quantified as vessel length density (VLD): i.e., the total vessel length in the area of each measured field (n = 5–10 fields per group); ***P < 0.001, **P < 0.01 vs. negative control (NC).

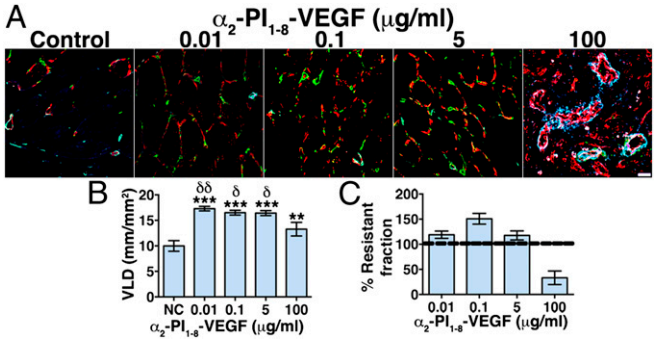

Fig. 3. Long-term stability of normal, but not aberrant, angiogenesis induced by optimized delivery of fibrin-bound α_2-PI_{1-8}-$VEGF_{164}$. Fibrin gels containing 56 μg/mL aprotinin-α_2-PI_{1-8} and 0 μg/mL (negative control), 0.01 μg/mL, 0.1 μg/mL, 5 μg/mL, and 100 μg/mL α_2-PI_{1-8}-$VEGF_{164}$ were injected into gastrocnemius muscles of SCID mice. Tissues were analyzed 3 mo later. (*A*) Frozen sections were immunostained to detect endothelial cells (CD31, in red), pericytes (NG2, in green), and smooth-muscle cells (α-SMA, in cyan). $n = 3$. (Scale bar: 20 μm.) (*B*) The amount of angiogenesis was quantified as vessel length density (mean VLD ± SEM; $n = 5$–10 fields per group); $^{***}P < 0.001$ or $^{**}P < 0.01$ vs. negative control, $^{\delta\delta}P < 0.01$, $^{\delta}P < 0.05$ vs. the 100 μg/mL condition. (*C*) The stabilization rate of vessels induced in each condition was calculated as the percentage ratio between VLD 3 mo and 4 wk after gel injection (% Resistant fraction), with a value of 100% or higher indicating complete stabilization and a value lower than 100% indicating vascular regression between the two time points.

An empty gel of the same composition was used as a negative control. Histological analysis (Fig. 4*A*) and VLD quantification (Fig. 4*C*) showed that, after 4 wk, 0.5 μg/mL α_2-PI_{1-8}-$VEGF_{164}$ promoted the growth of an abundant network of morphologically normal and mature capillaries, associated with $NG2^+/SMA^-$ pericytes, compared with negative control. However, contrary to the results in normal muscle, 5 μg/mL α_2-PI_{1-8}-VEGF led to a lower increase in VLD (Fig. 4*C*) and actually caused the growth of aberrant angioma-like structures, devoid of pericytes, and encompassed by smooth-muscle cells (asterisk in Fig. 4*A*). Blood flow was recorded by laser Doppler imaging both in the ischemic and nonoperated contralateral leg preoperatively, immediately after surgery and 7 d and 28 d later. To account for variables, including ambient light and temperature, calculated perfusion was expressed as a ratio of that in the ischemic to normal limb, as previously described (24). Blood flow in ischemic muscles was unaffected by 5 μg/mL α_2-PI_{1-8}-$VEGF_{164}$ compared with control (Fig. 4 *B* and *D*) but was significantly improved by 0.5 μg/mL α_2-PI_{1-8}-$VEGF_{164}$ after 4 wk compared with both control and 5 μg/mL VEGF (Fig. 4 *B* and *D*). Consistent with the improvement in blood flow, after 4 wk, the 0.5 μg/mL α_2-PI_{1-8}-$VEGF_{164}$ condition also significantly increased the number of histologically visible collateral arteries in the cranial part of the adductor thigh muscles compared with both other treatments (Fig. 4*E*).

To determine the general applicability of this approach, we further investigated whether the optimized delivery of fibrin-bound α_2-PI_{1-8}-$VEGF_{164}$ could promote functional improvement in a distinct ischemic wound-healing model. Based on the results described in Fig. 4, showing that the threshold between normal and aberrant angiogenesis in ischemic tissue lies between 0.5 μg/mL and 5 μg/mL α_2-PI_{1-8}-$VEGF_{164}$, a concentration of 2 μg/mL was used in the optimized fibrin-matrix composition as the therapeutic condition, with an empty gel of the same composition as negative control. Histological analysis (Fig. S8 *A* and *B*) and VLD quantification (Fig. S8 *C* and *E*) showed that, after 7 d, treatment with α_2-PI_{1-8}-$VEGF_{164}$ significantly increased dermis vascularization both in nonischemic and ischemic wounds. Microvessels were associated with $NG2^+$ pericytes in all groups (Fig. S8 *A* and *B*). Furthermore, α-SMA^+ mural cells were found associated with both microvessels and small-caliber arterioles and venules (arrowheads in Fig. S8 *A* and *B*) because, contrary to muscle tissue, in the skin, a proportion of capillary pericytes also express α-SMA (25). The α_2-PI_{1-8}-$VEGF_{164}$–treated tissues displayed a greater density of regularly shaped larger vessels (>15 μm) with the features of arterioles (covered by a regular smooth-muscle layer and homogeneous in size), consistently with the previously described effect of VEGF to cause arteriolization of preexisting vessels (26). Laser Doppler imaging showed that the increased vessel density in the α_2-PI_{1-8}-$VEGF_{164}$–treated wounds correlated with significantly improved tissue perfusion both in the nonischemic and ischemic sites by 7 d (Fig. S8 *D*, *F*, and *G*) ($P < 0.05$).

To evaluate the functional effects of increased angiogenesis and perfusion in the treated tissues, wound healing was analyzed. Under nonischemic conditions (Fig. S9*A*), the control-treated tissues showed signs of very mild inflammation with hyper/parakeratosis, without clearly identifiable dermis beneath the epidermis and with bleeding areas. The underlying muscle layer was fully infiltrated by inflammatory cells, and several muscle fibers displayed signs of partial necrosis, evidenced by infiltration of mononuclear inflammatory cells inside the myofibers. α_2-PI_{1-8}-$VEGF_{164}$ treatment slightly reduced epidermal hyperplasia, above which a layer of keratinized tissue with several apoptotic bodies was visible, whereas the stratus corneum was partially present, indicating that the α_2-PI_{1-8}-$VEGF_{164}$–treated tissue had reached a more advanced stage of regeneration of the physiological skin structure. Further, α_2-PI_{1-8}-$VEGF_{164}$ treatment reduced the inflammatory infiltrate in the underlying muscle layer and completely prevented myofiber damage. Under ischemic conditions

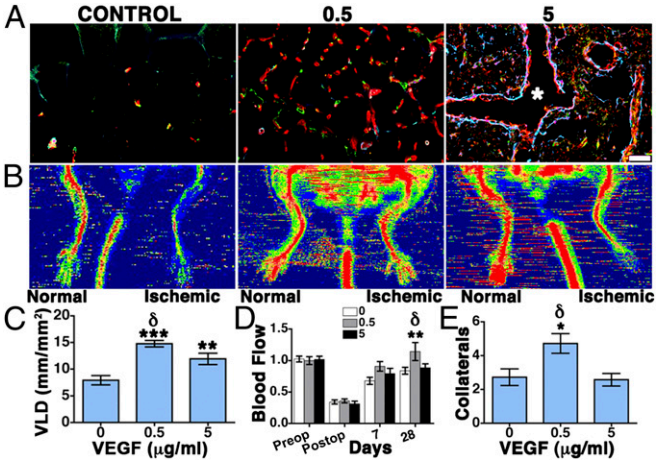

Fig. 4. Functional improvement of hind-limb ischemia by α_2-PI_{1-8}-$VEGF_{164}$. Fibrin gels containing 56 μg/mL aprotinin-α_2-PI_{1-8} and 0 μg/mL (negative control), 0.5 μg/mL, and 5 μg/mL α_2-PI_{1-8}-$VEGF_{164}$ were injected into the lower thigh muscles. Tissues were analyzed 4 wk later. (*A*) Frozen sections were immunostained to detect endothelial cells (CD31, in red), pericytes (NG2, in green), and smooth-muscle cells (α-SMA, in cyan). $n = 3$. (Scale bar: 20 μm.) (*B*) Representative laser Doppler images of nonischemic and ischemic limbs (left and right side of each image, respectively) 28 d after treatment with control gels (control) or 0.5 μg/mL and 5 μg/mL α_2-PI_{1-8}-$VEGF_{164}$. (*C*) The amount of angiogenesis was quantified as vessel length density (mean VLD ± SEM; $n = 5$–10 fields per group); $^{***}P < 0.001$ and $^{**}P < 0.01$ vs. negative control, $^{\delta}P < 0.05$ vs. the 0.5 μg/mL condition. (*D*) Blood flow was measured by laser Doppler imaging before surgery (preop) to set the baseline, immediately after (postop) and 7 and 28 d later. Results were expressed as the ratio between measured flow in the ischemic and the contralateral nonoperated hind limb. (*E*) The number of collateral arteries was determined histologically in the adductor muscles after 4 wk (mean ± SEM per field; $n = 5$–10 fields per group); $^{*}P < 0.05$ vs. negative control, $^{\delta}P < 0.05$ vs. the 0.5 μg/mL condition.

(Fig. S9*B*), control tissues displayed moderate hyperplasia of the epidermis, which was covered with a thick keratinized tissue full of apoptotic bodies. Both the dermis and the underlying muscle layer were prominently infiltrated with inflammatory cells, the muscle fibers were completely disorganized, many were invaded by monocytes, and several degenerative vacuoles were visible within the muscle layer. However, in the α_2-PI_{1-8}-$VEGF_{164}$–treated wounds, both epidermal hyperplasia and the thickness of the keratinized tissue with apoptotic bodies were reduced compared with controls. Further, α_2-PI_{1-8}-$VEGF_{164}$ treatment reduced the inflammatory infiltrate in the muscle layer and prevented myofiber damage, avoiding tissue necrosis. Therefore, histological analysis showed that treatment with α_2-PI_{1-8}-$VEGF_{164}$ significantly improved tissue regeneration and restoration of the physiological structure. Consistently, the quantification of wound-healing rate showed that α_2-PI_{1-8}-$VEGF_{164}$ promoted a significant acceleration of ischemic wound closure 7 d after gel implantation (Fig. S9*D*). Nonischemic wounds were also smaller both 3 d and 7 d after α_2-PI_{1-8}-$VEGF_{164}$ treatment although the differences were not statistically significant (Fig. S9*C*).

Discussion

Here, we found that the combination of fibrin-bound α_2-PI_{1-8}-$VEGF_{164}$ with the fibrin-bound fibrinolysis inhibitor aprotinin-α_2-PI_{1-8} provides a highly tunable platform to precisely control the VEGF dose delivered to tissues and efficiently induce stable and functional angiogenesis. Incorporation of aprotinin-α_2-PI_{1-8} at an optimal concentration is a key requirement to efficiently induce normal angiogenesis in vivo through its control of fibrinolysis and thus release of $\alpha_2PI_{1-8}VEGF_{164}$. Although differing release rates of the same α_2-PI_{1-8}-$VEGF_{164}$ concentration could cause disparate effects, from none to aberrant angiogenesis, optimal gel degradation rates enabled fibrin-bound α_2-PI_{1-8}-$VEGF_{164}$ to reliably induce exclusively normal, mature, stable, and functionally perfused microvascular networks over a 500-fold range of concentrations in normal muscle tissue. Remarkably, newly induced vessels did not regress for at least 3 mo whereas the implanted gels were almost completely consumed by 4 wk, demonstrating that they achieved independence from exogenous VEGF signaling for their survival and suggesting that they could persist indefinitely. This finding is particularly relevant for the therapeutic potential of this approach because one of the main limitations of recombinant protein delivery for therapeutic angiogenesis has been the insufficient duration of factor release to achieve persistent effects (20). On the other hand, aberrant angiogenesis induced by 100 μg/mL α_2-PI_{1-8}-$VEGF_{164}$ failed to recruit physiological pericyte coverage by 4 wk, when gel-bound factor was still present, consistently with the described function of VEGF as a negative regulator of pericyte function through formation of nonfunctional VEGFR-2/PDGFR-β complexes and consequent inhibition of PDGFR-β phosphorylation (27). When exogenous α_2-PI_{1-8}-VEGF-A_{164} became exhausted, more than 60% of the vascular structures induced by this high dose disappeared, indicating that they could not stabilize despite sustained VEGF release for at least 4 wk.

Therefore, incorporation of 56 μg/mL aprotinin-α_2-PI_{1-8} ensured an optimal gel degradation rate in vivo, which is the key parameter controlling both the duration and the effective dose of factor delivery. Under these optimized conditions, the angiogenic outcome was solely controlled by α_2-PI_{1-8}-$VEGF_{164}$ concentration, with aberrant vascular structures being induced by levels ≥25 μg/mL and physiological functional capillary networks resulting from a wide range of doses 0.01–5 μg/mL. The high tunability of the fibrin-bound delivery platform allowed us to span an extremely wide range of VEGF doses, including those determining the transition between normal and aberrant angiogenesis, which is a key feature for the design of preclinical dose-escalation studies. It should be noted that we chose to deliver the syngenic mouse recombinant factor $mVEGF_{164}$ instead of the clinically used human homolog $hVEGF_{165}$ because the experiments were performed in a mouse model and we recently found that the dose-dependent effects of VEGF are species-specific (28).

The concentration of α_2-PI_{1-8}-$VEGF_{164}$ did not affect the amount of induced vasculature because already the lowest dose caused the maximum increase in VLD, which was maintained over a 500-fold range. However, the dose of α_2-PI_{1-8}-$VEGF_{164}$ influenced the size of induced vessels, which remained unaffected by concentrations up to 0.1 μg/mL but was significantly increased by 5 μg/mL. These results are relevant for the therapeutic potential of α_2-PI_{1-8}-$VEGF_{164}$ delivery. In fact, we and others have previously shown that the size of newly induced vessels is key to determine the efficacy of therapeutic angiogenesis approaches (29, 30) as a similar increase in number without increase in size provided no therapeutic benefit (29). Based on these considerations, two different α_2-PI_{1-8}-$VEGF_{164}$ concentrations in the upper range of normal angiogenesis, 0.5 μg/mL and 5 μg/mL, were chosen to investigate dose-dependent functional improvement in a hind-limb ischemia model. Results showed that 0.5 μg/mL was effective to induce functional improvement as it caused a twofold increase in the amount of normal capillaries and significantly increased blood flow in ischemic tissue compared with controls. However, 5 μg/mL α_2-PI_{1-8}-$VEGF_{164}$, which induced only normal and stable angiogenesis in nonischemic muscle, actually stimulated the growth of aberrant vascular structures that failed to improve blood flow and collateral arteriogenesis in ischemic tissue. This disparate effect of the same concentration of α_2-PI_{1-8}-$VEGF_{164}$ may be attributable to the elevated levels of inflammatory cells and proteases during ischemia, which accelerate gel degradation and thus the effective rate of growth factor release. These results highlight the need to determine the therapeutic window of fibrin-bound α_2-PI_{1-8}-$VEGF_{164}$ delivery specifically for each envisioned clinical application as the unique biological variables associated with different pathologies can influence the effective degradation rate, factor release, and angiogenic outcome.

Considering the results obtained in the normal and ischemic hind limb, a concentration of 2 μg/mL was chosen to test the functional efficacy of fibrin-bound α_2-PI_{1-8}-$VEGF_{164}$ in an ischemic wound-healing model. The treatment with α_2-PI_{1-8}-$VEGF_{164}$ stimulated an 80% increase in normal angiogenesis, which significantly improved tissue perfusion both in nonischemic and ischemic tissues. The angiogenic stimulus induced a significant improvement of the wound closure in ischemic conditions and a positive trend toward improvement in nonischemic tissues. Interestingly, in control conditions, ischemia significantly slowed wound healing compared with normal tissue (55% vs. 38% still-open wound size by 7 d), and α_2-PI_{1-8}-$VEGF_{164}$ treatment restored healing in ischemia to the nonischemic level (36% still-open wound size by 7 d). In nonischemic tissue, α_2-PI_{1-8}-$VEGF_{164}$ treatment provided a further benefit (28% still-open wound size by 7 d), but the magnitude of the difference was insufficient to reach statistical significance. These data suggest that, in the absence of ischemia, tissue repair proceeds already at physiological speed and that increased blood flow could improve it only marginally whereas, in ischemic conditions, impaired perfusion is the critical factor limiting wound healing, and α_2-PI_{1-8}-$VEGF_{164}$ treatment may unfold its therapeutic effect. Consistently with this concept, it has been previously found that skin wounding in normal conditions leads to a transient localized ischemia due to microvascular damage and a six- to sevenfold up-regulation of endogenous VEGF expression, but this up-regulation is not further increased if wounding is carried out under conditions of ischemia (31).

In ischemic tissue, maximum blood supply is limited, and the opening of collateral arteries (arteriogenesis) is required to restore physiological flow levels to meet the metabolic demands of

regenerating tissue. Microvascular angiogenesis by VEGF can induce arteriogenesis by increasing blood flow and shear stress (1) and generating upstream responses through retrograde conduction along vessel walls via intercellular gap junctions (2). However, in chronic ischemia, spontaneous angiogenesis is insufficient to restore physiological flow, and we have previously found that VEGF doses higher than the maximal up-regulation achieved by the endogenous response are necessary to significantly increase both the amount and size of microvascular networks, induce collateral arteriogenesis, and achieve therapeutic benefit (29). Our results suggest that such doses can be effectively achieved in ischemic tissue by optimized delivery of fibrin-bound α_2-PI_{1-8}-$VEGF_{164}$. However, as the specific conditions prevalent in different tissues and pathologic states dictate the actual degradation rate and therefore the effective growth factor release in vivo, it is impossible to define a general therapeutic window. In this respect, the high tunability of the optimized platform developed in this study, with normal and stable angiogenesis being induced in healthy skeletal muscle over a 500-fold range of α_2-PI_{1-8}-$VEGF_{164}$ concentrations, provides a key enabling tool for specific dose-finding studies for each envisioned clinical application, such as peripheral or coronary artery disease, or chronic wounds, so that dosage can be carefully determined and adapted.

Methods

Detailed information is provided in *SI Methods*.

Recombinant α_2-PI_{1-8}-$VEGF_{164}$ Production and Purification. The transglutaminase substrate sequence NQEQVSPL (α_2-PI_{1-8}) was fused to the N terminus of the mouse VEGF-A_{164} cDNA by PCR. The fusion protein was expressed into *Escherichia coli* strain BL21 (Dε3) pLys (Novagen) and isolated as described previously (32) and in *SI Methods*.

Intramuscular Fibrin-Gel Implantation. Fifty microliters of fibrin hydrogel, prepared as described in *SI Methods*, was aspirated with an insulin syringe with integrated 30G needle (Becton Dickinson) and injected into the gastrocnemius muscle of 6- to 8-wk-old immunodeficient SCID CB.17 mice (Charles River), previously anesthetized by 3% isofluorane inhalation.

Hind-Limb Ischemia. Hind-limb ischemia experiments were performed on female CD1-mice (Charles River) by unilateral femoral artery ligation and excision, as detailed in *SI Methods*. Blood flow was measured by a laser Doppler imaging system (Moor Instruments), and results were presented as a ratio of the flow in the ischemic to that in the contralateral normally perfused hind limbs to account for variables, including ambient light and temperatures, as previously described (24) and as detailed in *SI Methods*.

Ischemic Wound Healing. An ischemic wound-healing model was performed on male Sprague–Dawley rats (Harlan-Winkelmann; $n = 6$ per group), based on a modification of a previously described epigastric flap model (33) and as detailed in *SI Methods*.

ACKNOWLEDGMENTS. We thank Celine Dessibourg (Ecole Polytechnique Fédérale de Lausanne) for preparation of the recombinant proteins and Sabine Pfeifer, Tatjana Morton, and the technical staff at the Ludwig Boltzmann Institute for invaluable assistance with in vivo imaging and wound-healing experiments. This work was supported in part by Swiss National Science Foundation Grants 127426 and 143898 (to A.B.) and by European Union FP7 Grant ANGIOSCAFF (CP-IP 214402) (to A.B., J.A.H., H.R., and M.E.).

1. Rissanen TT, et al. (2005) Blood flow remodels growing vasculature during vascular endothelial growth factor gene therapy and determines between capillary arterialization and sprouting angiogenesis. *Circulation* 112(25):3937–3946.
2. Pries AR, Höpfner M, le Noble F, Dewhirst MW, Secomb TW (2010) The shunt problem: Control of functional shunting in normal and tumour vasculature. *Nat Rev Cancer* 10(8):587–593.
3. Carmeliet P, Jain RK (2011) Molecular mechanisms and clinical applications of angiogenesis. *Nature* 473(7347):298–307.
4. Gupta R, Tongers J, Losordo DW (2009) Human studies of angiogenic gene therapy. *Circ Res* 105(8):724–736.
5. Ylä-Herttuala S, Markkanen JE, Rissanen TT (2004) Gene therapy for ischemic cardiovascular diseases: Some lessons learned from the first clinical trials. *Trends Cardiovasc Med* 14(8):295–300.
6. Karvinen H, Ylä-Herttuala S (2010) New aspects in vascular gene therapy. *Curr Opin Pharmacol* 10(2):208–211.
7. Ozawa CR, et al. (2004) Microenvironmental VEGF concentration, not total dose, determines a threshold between normal and aberrant angiogenesis. *J Clin Invest* 113(4):516–527.
8. Park JE, Keller GA, Ferrara N (1993) The vascular endothelial growth factor (VEGF) isoforms: Differential deposition into the subepithelial extracellular matrix and bioactivity of extracellular matrix-bound VEGF. *Mol Biol Cell* 4(12):1317–1326.
9. Dor Y, et al. (2002) Conditional switching of VEGF provides new insights into adult neovascularization and pro-angiogenic therapy. *EMBO J* 21(8):1939–1947.
10. Tafuro S, et al. (2009) Inducible adeno-associated virus vectors promote functional angiogenesis in adult organisms via regulated vascular endothelial growth factor expression. *Cardiovasc Res* 83(4):663–671.
11. Tayalia P, Mooney DJ (2009) Controlled growth factor delivery for tissue engineering. *Adv Mater* 21(32-33):3269–3285.
12. Banfi A, von Degenfeld G, Blau HM (2005) Critical role of microenvironmental factors in angiogenesis. *Curr Atheroscler Rep* 7(3):227–234.
13. Breen A, O'Brien T, Pandit A (2009) Fibrin as a delivery system for therapeutic drugs and biomolecules. *Tissue Eng Part B Rev* 15(2):201–214.
14. Schense JC, Bloch J, Aebischer P, Hubbell JA (2000) Enzymatic incorporation of bioactive peptides into fibrin matrices enhances neurite extension. *Nat Biotechnol* 18(4):415–419.
15. Schense JC, Hubbell JA (1999) Cross-linking exogenous bifunctional peptides into fibrin gels with factor XIIIa. *Bioconjug Chem* 10(1):75–81.
16. Ehrbar M, et al. (2004) Cell-demanded liberation of VEGF121 from fibrin implants induces local and controlled blood vessel growth. *Circ Res* 94(8):1124–1132.
17. Schmoekel HG, et al. (2005) Bone repair with a form of BMP-2 engineered for incorporation into fibrin cell ingrowth matrices. *Biotechnol Bioeng* 89(3):253–262.
18. Lorentz KM, Yang L, Frey P, Hubbell JA (2012) Engineered insulin-like growth factor-1 for improved smooth muscle regeneration. *Biomaterials* 33(2):494–503.
19. Traub S, et al. (2013) The promotion of endothelial cell attachment and spreading using FNIII10 fused to VEGF-A165. *Biomaterials* 34(24):5958–5968.
20. Ehrbar M, et al. (2008) The role of actively released fibrin-conjugated VEGF for VEGF receptor 2 gene activation and the enhancement of angiogenesis. *Biomaterials* 29(11):1720–1729.
21. Lorentz KM, Kontos S, Frey P, Hubbell JA (2011) Engineered aprotinin for improved stability of fibrin biomaterials. *Biomaterials* 32(2):430–438.
22. Armulik A, Genové G, Betsholtz C (2011) Pericytes: Developmental, physiological, and pathological perspectives, problems, and promises. *Dev Cell* 21(2):193–215.
23. Masaki I, et al. (2002) Angiogenic gene therapy for experimental critical limb ischemia: Acceleration of limb loss by overexpression of vascular endothelial growth factor 165 but not of fibroblast growth factor-2. *Circ Res* 90(9):966–973.
24. Couffinhal T, et al. (1998) Mouse model of angiogenesis. *Am J Pathol* 152(6):1667–1679.
25. Sundberg C, et al. (2001) Glomeruloid microvascular proliferation follows adenoviral vascular permeability factor/vascular endothelial growth factor-164 gene delivery. *Am J Pathol* 158(3):1145–1160.
26. Springer ML, et al. (2003) Localized arteriole formation directly adjacent to the site of VEGF-induced angiogenesis in muscle. *Mol Ther* 7(4):441–449.
27. Greenberg JI, et al. (2008) A role for VEGF as a negative regulator of pericyte function and vessel maturation. *Nature* 456(7223):809–813.
28. Mujagic E, et al. (2013) Induction of aberrant vascular growth, but not of normal angiogenesis, by cell-based expression of different doses of human and mouse VEGF is species-dependent. *Hum Gene Ther Methods* 24(1):28–37.
29. von Degenfeld G, et al. (2006) Microenvironmental VEGF distribution is critical for stable and functional vessel growth in ischemia. *FASEB J* 20(14):2657–2659.
30. Korpisalo P, et al. (2011) Capillary enlargement, not sprouting angiogenesis, determines beneficial therapeutic effects and side effects of angiogenic gene therapy. *Eur Heart J* 32(13):1664–1672.
31. Corral CJ, et al. (1999) Vascular endothelial growth factor is more important than basic fibroblastic growth factor during ischemic wound healing. *Arch Surg* 134(2):200–205.
32. Zisch AH, Schenk U, Schense JC, Sakiyama-Elbert SE, Hubbell JA (2001) Covalently conjugated VEGF: Fibrin matrices for endothelialization. *J Control Release* 72(1-3):101–113.
33. Michlits W, Mittermayr R, Schäfer R, Redl H, Aharinejad S (2007) Fibrin-embedded administration of VEGF plasmid enhances skin flap survival. *Wound Repair Regen* 15(3):360–367.

Supporting Information

Sacchi et al. 10.1073/pnas.1404605111

SI Methods

Recombinant $\alpha_2PI_{1–8}$-$VEGF_{164}$ Production and Purification. The cDNA for mouse $VEGF\text{-}A_{164}$ was PCR-amplified using primers designed to allow for fusion of the transglutaminase substrate sequence NQEQVSPL, comprising the 8 N-terminal residues of α_2-plasmin inhibitor ($\alpha_2\text{-}PI_{1–8}$) onto the N terminus of the amplified cDNA before insertion into the expression vector pRSET (Invitrogen). The fusion protein was expressed in *Escherichia coli* strain BL21 (Dε3) pLys (Novagen). The recombinant $\alpha_2\text{-}PI_{1–8}\text{-}VEGF\text{-}A_{164}$ was isolated from inclusion bodies, processed, and refolded using a slightly modified version of a previously published protocol (1). Briefly, the inclusion bodies were collected from the bacterial lysate by centrifuging, washed with Triton X-114 to remove membrane proteins and endotoxins, and extracted with urea buffer overnight at 4 °C under magnetic stirring. Further dimerization of $\alpha_2\text{-}PI_{1–8}\text{-}VEGF\text{-}A_{164}$ was done with a redox system (0.5 mM oxidized glutathione, 5 mM reduced glutathione) added into the protein solution after the 2 M urea dialysis, and $\alpha_2\text{-}PI_{1–8}\text{-}VEGF\text{-}A_{164}$ was dimerized under stirring for 48 h at 4 °C. Then, glutathione and urea were removed by three sequential dialyses of 24 h against Tris buffers. Proteins were then concentrated using a 10-kDa Amicon tube (Millipore, Merck) and further filtered through a 0.22-μm filter. $\alpha_2PI_{1–8}\text{-}VEGF_{164}$ monomers and dimers were separated using size exclusion with a HiLoad 16/60 Superdex 75-pg column (GE healthcare). Fractions corresponding to $\alpha_2PI_{1–8}$-VEGF dimers were pooled together, concentrated with Amicon tubes, and filtered through a 0.22-μm filter. $\alpha_2PI_{1–8}$-VEGF dimers were verified to be >99% pure by SDS/PAGE and MALDI-TOF analysis. Endotoxin level was verified to be under 0.05 EU/mg of protein using the LAL assay (GenScript).

Fibrin-Gel Preparation. Fibrin matrices were prepared by mixing human fibrinogen (plasminogen-, von Willebrand Factor-, and fibronectin-depleted; Enzymes Research Laboratories), factor XIIIa (CSL Behring), and thrombin (Sigma-Aldrich) combined at different concentrations as described in *Results* with 2.5 mM Ca^{2+} in 4-(2-hydroxyethyl)-1-piperazineethanesulfonic acid (Hepes) (Lonza). Matrices containing aprotinin-$\alpha_2\text{-}PI_{1–8}$ [produced as described (2)] and $\alpha_2\text{-}PI_{1–8}\text{-}VEGF_{164}$ were obtained by adding the engineered proteins to the cross-linking enzymes solution before mixing with fibrinogen. Matrices were allowed to polymerize at 37 °C for 1 h before use or directly injected after mixing to allow in situ polymerization, depending on the experimental design.

$\alpha_2\text{-}PI_{1–8}\text{-}VEGF\text{-}A_{164}$ Release Profile from Fibrin Hydrogels. Fibrin matrices of 50 μL volume were generated with 10 mg/mL fibrinogen, 2 U/mL thrombin, 5 U/mL factor XIII, 5 mM calcium chloride as previously described for this assay (3), and 10 μg/mL $VEGF\text{-}A_{164}$ (R&D Systems) or of $\alpha_2\text{-}PI_{1–8}\text{-}VEGF_{164}$. Fibrin gels were polymerized at 37 °C for 1 h and transferred into 24-wells containing 500 μl of washing buffer. The 100% release control well contained only the growth factor in buffer. Every 24 h, buffers were collected, stored at −20 °C and replaced with fresh buffer. For the 100% release control well, 20 μl of buffer was taken out every day and stored at −20 °C. After 7 d, the cumulative release of growth factor was quantified by ELISA using the 100% released control as reference (DuoSet; R&D Systems).

VEGF-R2 Phosphorylation Assay. Human umbilical vein endothelial cells (HUVECs) (PromoCell) were seeded in 96-well plates (3,000 cells per well) and starved 4 h with serum-free MCDB-131 medium (Invitrogen). Cells were then stimulated with 50 ng/mL $VEGF\text{-}A_{164}$ or $\alpha_2\text{-}PI_{1–8}\text{-}VEGF\text{-}A_{164}$ for 5 min. Phosphorylated VEGF-R2 was quantified with a phospho-ELISA kit. Briefly, ELISA plates were coated with a capture antibody for VEGF-R2 and then incubated with cell lysates. The phosphorylation state was detected with an anti-phospho-tyrosine antibody and normalized to a standard according to manufacturer instructions (phospho-VEGF-R2/KDR, DuoSet IC; R&D Systems).

In Vitro Gel Polymerization. Fibrin matrices of 50 μL volume were prepared onto a plastic minitray (Nunc Microwell Minitrays; Sigma-Aldrich) and placed on ice to slow down gel polymerization. The fibrinogen solution was first deposited into the well with a pipette tip, avoiding the formation of bubbles, and the cross-linking enzyme solution was added. Solutions were mixed three times with the pipette to guarantee homogenous mixing. The start of polymerization was defined by the change of consistency from liquid to stiff as detected by touch with the pipette tip.

Rheology. Fibrin-gel discs of 1-mm thickness were preformed into press-to-seal silicone isolator slides (Invitrogen) coated with parafilm at room temperature. Gels were allowed to polymerize for 1 h at 37 °C, removed from the support, and placed in PBS overnight at 4 °C to allow swelling. Gel stiffness was determined by performing small-strain oscillatory shear rheometry using a Bohlin CVO 120 high-resolution rheometer with plate–plate geometry at room temperature (Instrumat SA). Gels were sandwiched between the two plates of the rheometer with compression up to 80% of their original thickness to avoid slipping. Measurements were then conducted in a constant strain (0.05) mode as a function of frequency (from 0.1 Hz to 10 Hz) to obtain dynamical spectra ($n = 3$ per condition).

Intramuscular Fibrin-Gel Implantation. To avoid an immunological response to human fibrinogen and cross-linking enzymes, 6- to 8-wk-old immunodeficient CB.17 SCID mice (Charles River Laboratories) were used. Animals were treated in accordance with the Swiss Federal guidelines for animal welfare, after approval from the Veterinary Office of the Canton of Basel-Stadt (Basel, Switzerland). A liquid volume of 50 μL was aspirated rapidly with a 0.3-mL insulin syringe with integrated 30 G needle (Becton Dickinson) and injected into the gastrocnemius muscle of the mice previously anesthetized with 3% isofluorane inhalation. After injection, in situ polymerization was allowed for 20 s before slowly extracting the needle.

In Vivo Multispectral Imaging. Fibrin gels were prepared as previously described, but fluorescent Alexa 647-conjugated fibrinogen (Invitrogen) was included at a concentration of 0.5 ng/mL to monitor the degradation of the different fibrin-gel compositions in vivo by noninvasive multispectral imaging. The experiments were performed at the Ludwig Boltzmann Institute after approval by the local ethical committee. Animals were treated according to the National Institutes of Health guidelines. Carprofen (2.5 mg/kg; Pfizer) was administered to animals preoperatively and for the following 3 d to ensure analgesia. A liquid volume of 50 μL was injected into gastrocnemius muscles on both hindlimbs of BALB/c nu/nu nude mice ($n = 10$ per group). The fluorescence of the fibrin matrix was noninvasively followed and quantified over a period of 9 d using a multispectral imaging system (Maestro Imaging System; CRI). Regions of interest were defined and analyzed. The signal (given as counts per s) was normalized to the values obtained on day 1 and expressed as a percentage.

Histological Analyses. Mice were anesthetized with Ketamin (100 mg/kg) and Xylazin (10 mg/kg) i.p. and euthanized by vascular perfusion of 1% paraformaldehyde (PFA) (Sigma-Aldrich) in PBS (pH 7.4) for 3 min under 120 mm/Hg of pressure. Gastrocnemius muscles were harvested, postfixed in 0.5% PFA in PBS (pH 7.4) for 2 h at room temperature, and cryoprotected in 30% (wt/vol) sucrose in PBS at 4 °C overnight. Muscles were embedded in optimal cutting temperature (OCT) compound (CellPath), frozen in freezing isopentane, and cryosectioned. Tissue sections were stained with H&E to verify the intramuscular localization of the gel. Vascular morphology was analyzed by immunofluorescence staining on 12-μm-thick frozen sections cut along the longitudinal axis. The following primary antibodies and dilutions were used: rat anti-mouse CD31 (clone MEC 13.3; BD Biosciences) at 1:100; mouse anti-human α-SMA (clone 1A4; Sigma-Aldrich) at 1:400; and rabbit anti-rat NG2 (Millipore, Merck) at 1:200. Fluorescently labeled secondary antibodies (Invitrogen) were used at 1:200. Fluorescence images were taken with a 40× objective on a Carl Zeiss LSM710 3-laser scanning confocal microscope (Carl Zeiss).

In some experiments, the amount of nondegraded gel was assessed histologically by immunostaining with a primary antibody that specifically recognizes fibrin, but not fibrinogen (mouse anti-human fibrin, clone E8; Beckman Coulter Immunotech) at a dilution of 1:200. Tissue sections were obtained at 250-μm intervals, in three muscles per group ($n = 3$). Images were taken in each section where gel was detectable with a 10× objective on an Olympus BX61 fluorescence microscope (Olympus) and merged using the multiple image alignment (MIA) function of the CellP imaging analysis software (Olympus) to reconstruct the total area of the tissue section in which the nondegraded gel was present. The total surface area occupied by nondegraded gel was quantified (in mm^2) using ImageJ software (http://rsb.info.nih.gov/ij/) as the sum of all sections in each analyzed muscle.

In some experiments, physiological perfusion of induced vessels was assessed by intravascular staining with a fluorescently labeled *Lycopersicon esculentum* (tomato) lectin (Vector Laboratories) that binds the luminal surface of blood vessels, as previously described (4). Briefly, mice were anesthetized, and lectin was injected i.v. (50 μL of a 2 mg/mL lectin solution per mouse) and allowed to circulate for 4 min before vascular perfusion of 1% PFA in PBS (pH 7.4) for 3 min under 120 mm/Hg of pressure.

Vessel Measurements. Vessel diameters and vessel length density (VLD) were measured in muscle cryosections after immunostaining for CD31, NG2, and SMA as previously described (4, 5). Briefly, vessel diameters were measured by overlaying captured microscopic images with a square grid. Squares were selected randomly, and the diameter of each vessel, if present, in the defined square was measured (in μm). Around 500 total diameter measurements were obtained from three independent muscles for each group ($n = 3$). VLD was measured in 5–10 fields per muscle from three muscles per group ($n = 3$) by tracing the total length of vessels in each field and dividing it by the area of the field (mm of vessel length/mm^2 of surface area). All analyses were performed using the Cell P imaging software (Olympus).

Subcutaneous Fibrin-Gel Implantation. All animal procedures were approved by the Cantonal Veterinary Office of Canton Zurich (Zurich, Switzerland). Female Crl:CD1 Foxn1^{nu} nude mice were used at 4–5 wk of age. Gel implantation and excision was performed as described (6). Briefly, animals were anesthetized by inhalation of 2% isofluorane. The dorsal skin was disinfected with 70% ethanol. Two incisions, ∼1.5 cm long, were made along the left and right sides of the dorsum. Four gels of 20 μL volume were implanted in each mouse in a random order, a 10–0 Dafilon suture (Braun) was placed through each fibrin-gel pellet to fasten the gel to the s.c. area just beneath the skin, and wounds were closed with 7–0 Prolene sutures (Ethicon). Animals were euthanized 14 d later by carbon dioxide asphyxiation. Gels were excised together with the surrounding skin, and samples were stored at −80 °C for further analysis.

α_2-PI$_{1-8}$-VEGF-A$_{164}$ Protein Extraction and Quantification. The concentration of α_2-PI$_{1-8}$-VEGF$_{164}$ in the gels after in vivo implantation was measured from explanted and frozen fibrin gels as described (6). They were washed in PBS for 8 h at 4 °C, changing the PBS every hour. Afterward, 50 mU of plasmin (Sigma-Aldrich) in 50 μL of deionized water were added to each gel and incubated at 37 °C on a shaker at 1,000 rpm. After 8 h, the plasmin solution was renewed and incubation at 37 °C on a shaker continued until all gels were completely dissolved (∼48 h). The amount of VEGF in the resulting samples was measured using an ELISA kit (R&D Systems). One hundred microliters of each sample was used in triplicate, and the assay was performed according to the manufacturer's instructions.

Endothelial Cell Proliferation Assay. VEGF biological activity was assessed in a HUVEC proliferation assay as described (6). Cells were cultured in 96-well plates (5,000 cells per well) in EGM-2 fully supplemented growth medium (Lonza) in 5% CO_2 at 37 °C. Before the assay, cells were starved for 6 h with EBM-2 medium (Lonza) supplemented with 1% FCS. Stimulation was started by supplementing the EBM-2 medium with 50 ng of the α_2-PI$_{1-8}$-VEGF$_{164}$ liberated from the gels or 50 ng of recombinant mouse VEGF$_{164}$ (Peprotech) as a positive control. Cell numbers were determined 72 h later by adding 10 μl of cell proliferation reagent (WST-1; Roche) to each well. After 4 h of incubation, absorbance of the samples was measured at 650 nm using a microplate reader (Biotek).

Plasma-Leakage Measurements. Evans Blue assays were performed as described previously (5). Four weeks after gel implantation, Evans Blue dye (30 mg/kg of mouse body weight in 100 μL of PBS) (Sigma) was injected into the femoral vein. After 4 h, mice were perfused with 1% paraformaldehyde in 0.05 M citric acid (pH 3.5), and the gastrocnemius muscles were harvested and weighed. Evans Blue was extracted from tissue with formamide at 55 °C overnight and measured with a spectrophotometer at 610 nm. Plasma leakage was expressed as nanograms of extravasated dye per milligram of tissue wet weight ($n = 4$ per group).

Hind-Limb Ischemia Model and Analysis. Experiments were performed at the Ludwig Boltzmann Institute (Vienna), after approval by the local ethical committee. The hind-limb ischemia was performed on female CD1 mice ($n = 11$ per group), weighing 28–36 g (Charles River). Mice were anesthetized with isoflurane (2.5 vol %), and femoral artery ligation and excision were performed unilaterally according to a randomization protocol. Under a surgical microscope, the femoral artery was ligated proximally (inguinal ligament) and distally (bifurcation into saphenous and popliteal artery) and excised. The wound was closed using nonabsorbable sutures in a single-knot technique. The contralateral normally perfused hind limb of each animal served as an internal control. Gels containing either 0 μg/mL, 0.5 μg/mL, or 5 μg/mL α_2-PI$_{1-8}$-VEGF$_{164}$ were injected into the distal part of the quadriceps (50 μL), adductor (30 μL), and biceps femoris (30 μL) thigh muscles of mice according to a randomization protocol. As analgesic treatment, animals received 0.1 mg/kg buprenorphin preoperatively and 1.5 mg/kg meloxicam for the first 3 d after surgery. Hind-limb blood flow was measured by a laser Doppler imaging system (LDI) (Moor Instruments), preoperatively as baseline, postoperatively to assess effective induction of ischemia, and on days 7 and 28. Data analysis was performed with the Moor LDI image processing software (Version 5.3; Moor Instruments). The scan mode was set at 10 ms per pixel, and a resolution of 256 × 256

pixels was chosen. Blood flow was calculated as a ratio of that in the ischemic to that in the contralateral normally perfused hind limbs to account for variables, including ambient light and temperatures, as previously described (7). On day 28, mice were anesthetized with ketamine (67 mg/kg) and xylazine (13 mg/kg) i.p before intravascular systemic perfusion with 1% PFA in PBS (pH 7.4) for 3 min under 120 mm/Hg of pressure. The adductor, biceps, and quadriceps femoris muscles were harvested, postfixed in 0.5% PFA in PBS (pH 7.4) for 2 h at room temperature, cryoprotected in 30% (wt/vol) sucrose in PBS at 4 °C overnight, embedded in OCT compound (CellPath), frozen in freezing isopentane, and cryosectioned.

Tissue sections were analyzed to assess the intramuscular localization of the implanted gel, vessel morphology, and length density as described in *Histological Analyses* and *Vessel Measurements*. After serial sectioning of the entire adductor muscles, the number of collateral arteries was quantified on a single section from each sample, so as to avoid double counting, taken from the proximal part of the muscle in an area remote from the area of injection of the gel and where no angiogenesis was detectable. Collateral vessels >20 μm in diameter were quantified by costaining for CD31 and α-SMA as previously described (8) on three to six random fields per muscle, acquired with a 20× objective on an Olympus BX61 fluorescence microscope (Olympus). Results were expressed as collaterals per field of view ($n = 3$ muscles per group).

Ischemic Wound-Healing Model and Analysis. Experiments were performed at the Ludwig Boltzmann Institute (Vienna), after approval by the local ethical committee. An ischemic wound-healing model was performed on male Sprague–Dawley rats ($n =$ 6 per group), weighing 300–350 g (Harlan-Winkelmann), based on a modified epigastric flap model as previously described (9). Briefly, the rats were anesthetized with ketamine (110 mg/kg) and xylazine (12 mg/kg) i.p. A square skin flap of 8 cm by 8 cm was elevated from cranial to caudal and remained connected to blood circulation only at the caudal base. Half of the flap was rendered ischemic by ligating the left or right inferior neurovascular bundle, and the flap was sutured back. The flap was divided into three vertical zones of equal size, the outer zone on the ligation side reflecting ischemic tissue and the opposite one reflecting vital areas. A 1.5-cm-diameter circular wound was created within the elevated flap in the middle of each outer zone, thus resulting in an ischemic wound on one side and an internal control wound on the opposite side. A volume of 100 μL of optimized-composition gel with 56 μg/mL aprotinin-α_2-PI_{1-8}, either empty or containing 2 μg/mL α_2-PI_{1-8}-$VEGF_{164}$, was applied at the wound sites according to a randomization protocol, allowing solidification in situ. Wounds were covered with a transparent foil dressing (Opsite; Smith and Nephew) and fixed with a second dressing (Fixomull-stretch), changing them on day 1 and 3. As an analgesic treatment, rats received 1.25 mg/kg butorphanol and 0.15 mg/kg meloxicam s.c. on the day of surgery and 3 d later.

Superficial tissue perfusion was measured by a laser Doppler imaging system (Moor Instruments), preoperatively as baseline, postoperatively to assess effective induction of ischemia, and on days 3 and 7. Preoperative baseline values were set at 100%, and subsequent scans were normalized to these values and expressed as a percentage of baseline. The ischemic and nonischemic vertical zones were scanned and evaluated separately. The scan mode was set at 10 ms per pixel, and a resolution of 256 × 256 pixels was chosen. Analyses were made by a software evaluation tool provided with the LDI Moor system (Moor Instruments). Perfusion values were recorded as colored pixels, giving the color-coordinated 2D image of the flap perfusion.

Wound closure was evaluated by planimetric analysis. Excision wounds were traced on a transparent acrylic sheet postsurgery and at days 3 and 7. The sheets were photographed with adjacent standard ruler and analyzed by a planimetric software (Lucia G1, Version 4.8; Laboratory Imaging). The results were expressed as a percentage of the total postoperative wound surface area. On day 7, the animals were euthanized by an intracardiac injection of 150 mg/kg Pentobarbital, and the entire wound areas were excised. Tissues were fixed in 4% (wt/vol) neutral-buffered formalin for 24 h, dehydrated in ascending concentrations of alcohol, embedded in paraffin, and 4-μm-thick sections were cut on a rotary microtome. The samples were warmed to 60 °C for 30 min, deparaffinized in xylene, and rehydrated in graded alcohols. A blocking treatment (1% H_2O_2 in distilled water) to deactivate endogenous peroxidase was performed for 10 min. NG2 staining was performed with 1:100 rabbit anti-rat NG2 antibody (Millipore, Merck) overnight at 4 °C, without epitope retrieval. Samples were rinsed with Tris-buffered saline (TBS) for 5 min and incubated with anti-rabbit antibody labeled with biotin (Dako) for 1 h at room temperature, followed by staining with a biotin substrate kit (VECTASTAIN Elite ABC kit; Vector Labs).

Samples for von Willebrand Factor (vWF) antibody were pretreated with proteinase K (Dako) for 8 min whereas samples for SMA staining underwent heat-induced epitope retrieval for around 20 min at 95 °C in Tris-EDTA buffer (Zytomed). All slides were moved to immunostaining chambers (Coverplate System; Thermo Shandon) and washed with TBS for 5 min. The tissue sections were incubated with 1:100 vWF antibody (polyclonal rabbit anti-human, A0082; Dako) and with 1:5,000 SMA antibody (monoclonal mouse anti-human, A2547; Sigma-Aldrich) for 1 h at room temperature. After rinsing with TBS, anti-mouse or anti-rabbit HRP-labeled micropolymers (Dako) were applied to the slides for 30 min at room temperature, followed by staining with a peroxidase substrate kit (ImmPACT NovaRED; Vector Labs). The slides were then counterstained with hematoxylin, dehydrated, and mounted with Entellan mounting medium (Merck).

Statistics. Data are presented as mean ± SEM. The significance of differences was evaluated using analysis of variance (ANOVA) followed by the Bonferroni test (for multiple comparisons) or using a Mann–Whitney test (for single comparisons), and $P <$ 0.05 was considered statistically significant.

1. Zisch AH, Schenk U, Schense JC, Sakiyama-Elbert SE, Hubbell JA (2001) Covalently conjugated VEGF—fibrin matrices for endothelialization. *J Control Release* 72(1-3): 101–113.
2. Lorentz KM, Kontos S, Frey P, Hubbell JA (2011) Engineered aprotinin for improved stability of fibrin biomaterials. *Biomaterials* 32(2):430–438.
3. Ehrbar M, et al. (2004) Cell-demanded liberation of VEGF121 from fibrin implants induces local and controlled blood vessel growth. *Circ Res* 94(8):1124–1132.
4. von Degenfeld G, et al. (2006) Microenvironmental VEGF distribution is critical for stable and functional vessel growth in ischemia. *FASEB J* 20(14):2657–2659.
5. Ozawa CR, et al. (2004) Microenvironmental VEGF concentration, not total dose, determines a threshold between normal and aberrant angiogenesis. *J Clin Invest* 113(4): 516–527.
6. Largo RA, et al. (2014) Long-term biostability and bioactivity of "fibrin linked" VEGF121 in vitro and in vivo. *Biomater. Sci.* 2(4):581–590.
7. Couffinhal T, et al. (1998) Mouse model of angiogenesis. *Am J Pathol* 152(6): 1667–1679.
8. Heeschen C, et al. (2001) Nicotine stimulates angiogenesis and promotes tumor growth and atherosclerosis. *Nat Med* 7(7):833–839.
9. Michlits W, Mittermayr R, Schäfer R, Redl H, Aharinejad S (2007) Fibrin-embedded administration of VEGF plasmid enhances skin flap survival. *Wound Repair Regen* 15 (3):360–367.

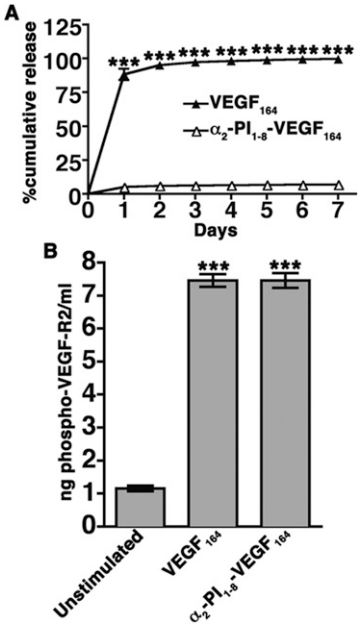

Fig. S1. Characterization of the fusion protein α_2-$PI_{1–8}$-$VEGF_{164}$. (*A*) Percent cumulative release of α_2-$PI_{1–8}$-$VEGF_{164}$ and native $VEGF_{164}$ from fibrin gels. The quantity of native and variant $VEGF_{164}$ was measured on buffer collected and replaced daily for 7 d by ELISA. Values are reported as mean ± SEM ($n = 3$). (*B*) Phosphorylation assay. Serum-starved HUVECs were incubated with 50 ng/mL native $VEGF_{164}$ or α2-PI_{1-8}-$VEGF_{164}$, and the amount of phosphorylated VEGF-Receptor 2 (VEGF-R2) was quantified by ELISA (ng/mL). Values are reported as mean ± SEM ($n = 3$); ***$P < 0.001$.

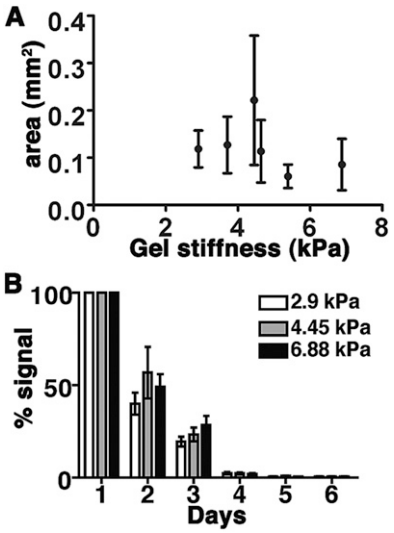

Fig. S2. In vivo gel degradation. (*A*) Gel compositions of different stiffness were injected into the gastrocnemius muscles of SCID mice. Immunofluorescence staining of serial tissue sections with a fibrin-specific antibody showed no significant differences in the amount of remaining gel 4 d after injection. Results are shown as mean gel area (mm^2) ± SEM ($n = 3$). (*B*) Different gel compositions spanning the whole range of stiffnesses were prepared with fluorescently labeled fibrinogen and injected into gastrocnemius muscles. The degradation was monitored in vivo daily for a period of 9 d by noninvasive imaging of fibrin fluorescence. Results are shown as percentage of the initial fluorescent signal remaining over time (mean ± SEM; $n = 9$).

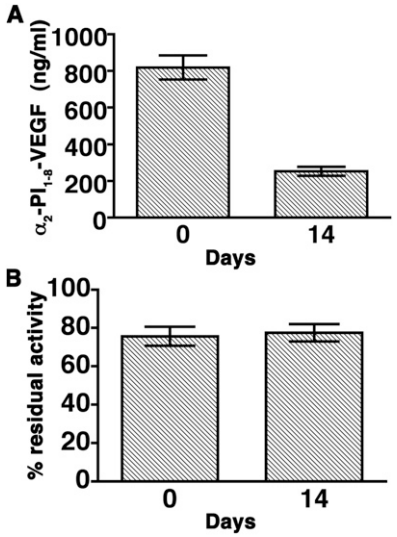

Fig. S3. The biological activity of α_2-PI$_{1-8}$-VEGF$_{164}$ is preserved after 2 wk of in vivo implantation. Fibrin gels of 20 μL volume containing 100 μg/mL α_2-PI$_{1-8}$-VEGF$_{164}$ and 56 μg/mL aprotinin-α_2-PI$_{1-8}$ were preformed in vitro and frozen at −80 °C either immediately (day 0) or 2 wk after s.c. implantation into nude mice (day 14). (*A*) After digestion with plasmin for ∼56 h at 37 °C, the amount of extracted α_2-PI$_{1-8}$-VEGF$_{164}$ was measured by ELISA. Results are shown as mean concentration in the extraction supernatant (ng/mL) ± SEM (n = 4). (*B*) The biological activity of the extracted α_2-PI$_{1-8}$-VEGF$_{164}$ was determined in a HUVEC proliferation assay. Recombinant fresh VEGF$_{164}$ was used as positive control. Results are shown as the percentage residual activity in cell proliferation compared with fresh recombinant VEGF, set at 100% (mean ± SEM; n = 4).

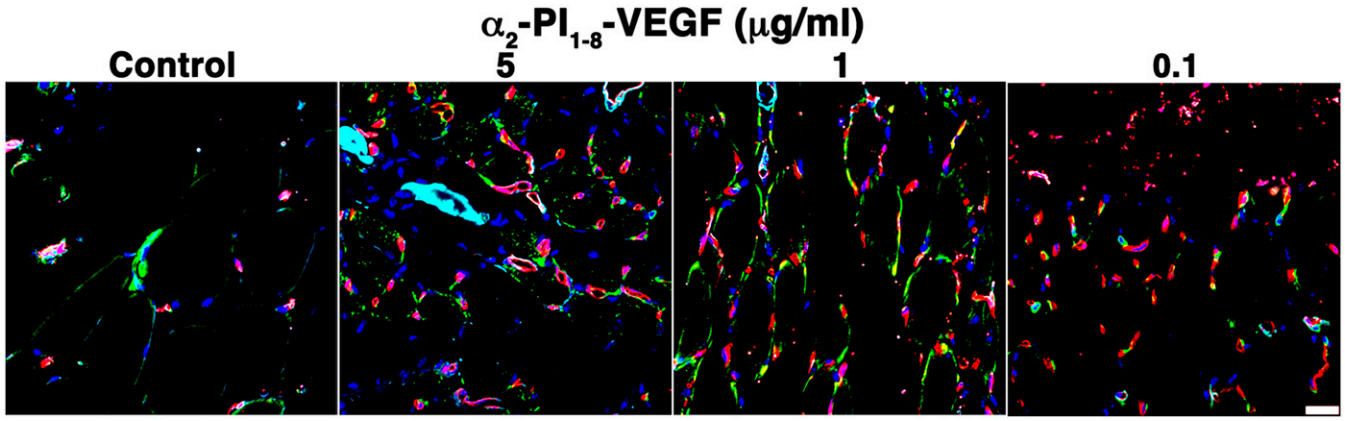

Fig. S4. A wide range of α_2-PI$_{1-8}$-VEGF$_{164}$ doses induces robust and normal angiogenesis. Fibrin gels containing 56 μg/mL aprotinin-α_2-PI$_{1-8}$ and 0 μg/mL (negative control), 5 μg/mL, 1 μg/mL, or 0.1 μg/mL α_2-PI$_{1-8}$-VEGF$_{164}$ were injected into the gastrocnemius muscles of SCID mice. Tissues were analyzed 9 d later, and frozen sections were immunostained to detect endothelial cells (CD31, in red), pericytes (NG2, in green), smooth-muscle cells (α-SMA, in cyan), and nuclei (DAPI, in blue). n = 3. (Scale bar: 20 μm.)

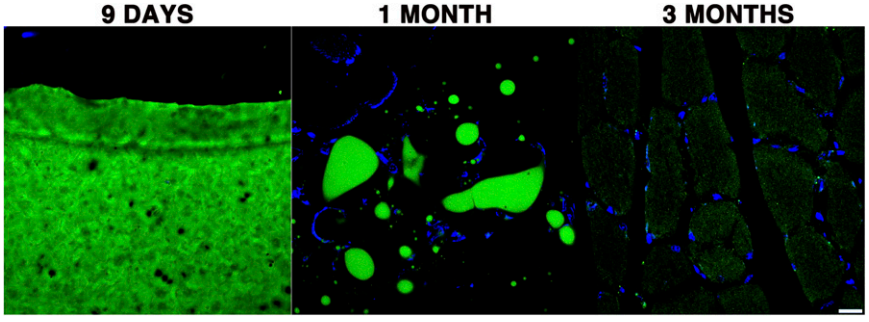

Fig. S5. In vivo persistence of optimized fibrin gels. Fibrin gels containing 56 μg/mL aprotinin-α_2-PI$_{1-8}$ and 0.1 μg/mL α_2-PI$_{1-8}$-VEGF$_{164}$ were injected into the gastrocnemius muscles of SCID mice. Tissues were analyzed 9 d, 1 mo, or 3 mo later, and frozen sections were immunostained to detect fibrin (anti-fibrin antibody, in green) and nuclei (DAPI, in blue). Abundant gel is visible 9 d after injection whereas, after 4 wk, small residues are still present and none is detectable after 3 mo. (Scale bar: 20 μm.)

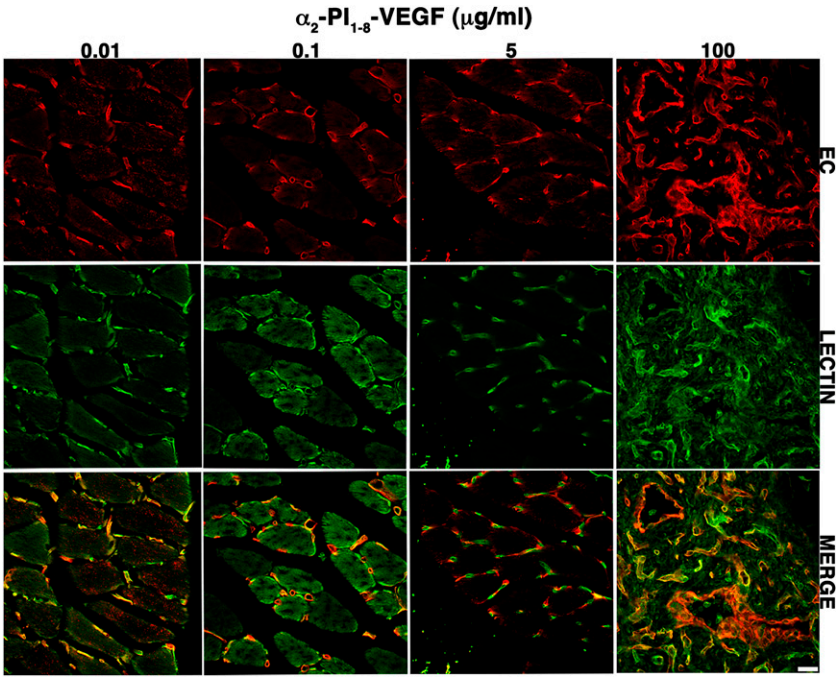

Fig. S6. Vessels induced by α_2-$PI_{1–8}$-$VEGF_{164}$ are functionally perfused after 4 wk. Fibrin gels containing 56 μg/mL aprotinin-α_2-$PI_{1–8}$ and 0.01 μg/mL, 0.1 μg/mL, 5 μg/mL, and 100 μg/mL α_2-$PI_{1–8}$-$VEGF_{164}$ were injected into gastrocnemius muscles of SCID mice. FITC-lectin was injected i.v. into mice 4 wk later, just before euthanizing. Endothelial structures (EC) were stained with an antibody against CD31 (red) whereas FITC-lectin is shown in green. Perfused vessels were identified as staining positive for both CD31 and FITC-lectin. $n = 3$. (Scale bar: 20 μm.)

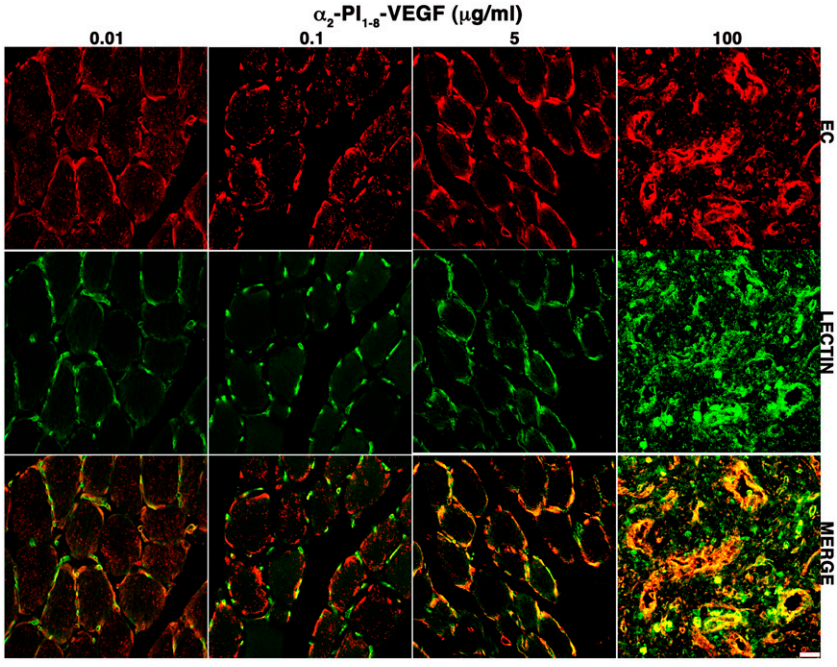

Fig. S7. Vessels induced by α_2-$PI_{1–8}$-$VEGF_{164}$ are functionally perfused after 3 mo. Fibrin gels containing 56 μg/mL aprotinin-α_2-$PI_{1–8}$ and 0.01 μg/mL, 0.1 μg/mL, 5 μg/mL, and 100 μg/mL α_2-$PI_{1–8}$-$VEGF_{164}$ were injected into gastrocnemius muscles of SCID mice. FITC-lectin was injected i.v. into mice 3 mo later, just before euthanizing. Endothelial structures (EC) were stained with an antibody against CD31 (red) whereas FITC-lectin is shown in green. Perfused vessels were identified as staining positive for both CD31 and FITC-lectin. $n = 3$. (Scale bar: 20 μm.)

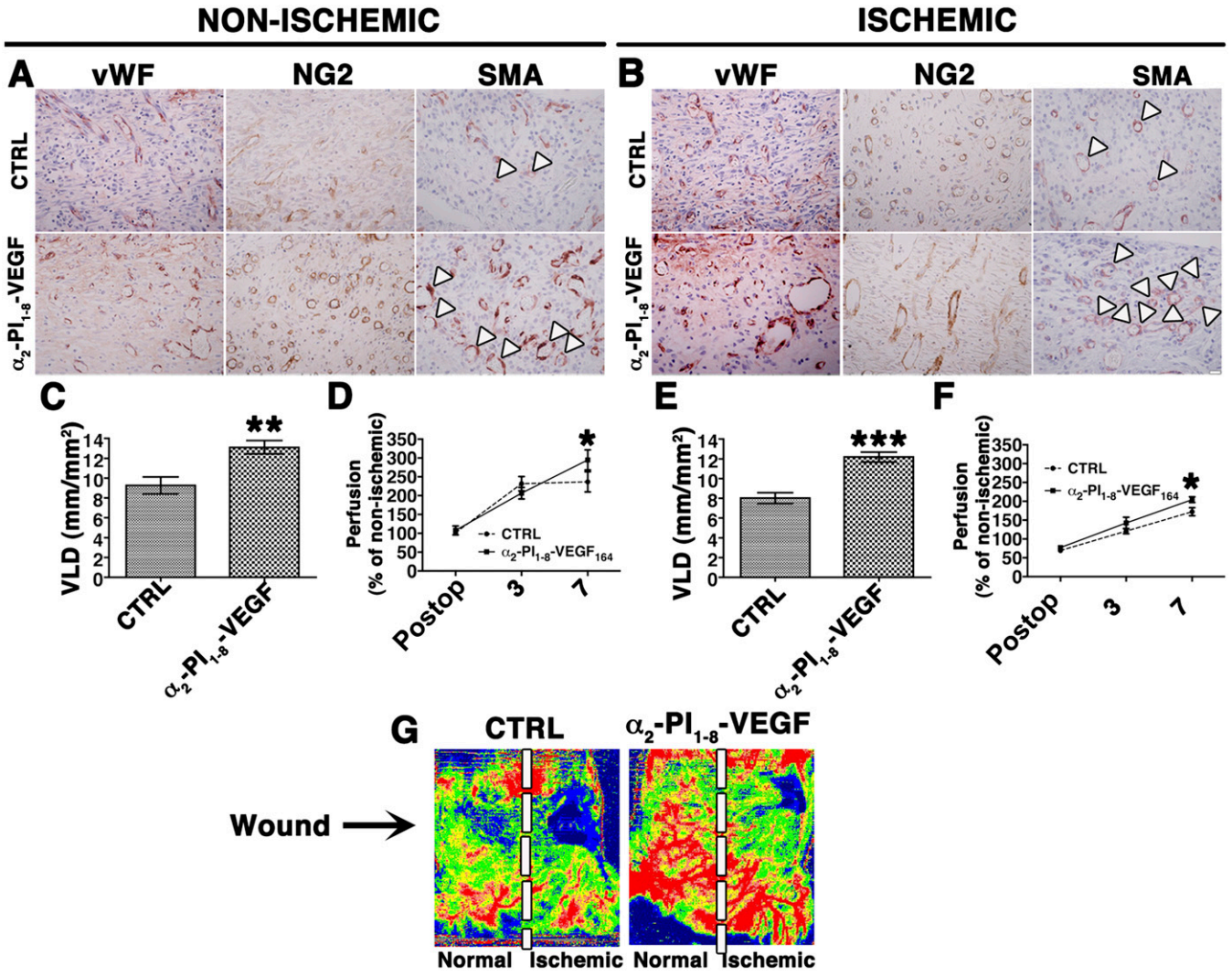

Fig. S8. α_2-PI$_{1-8}$-VEGF$_{164}$ significantly improves angiogenesis and tissue perfusion in an ischemic wound-healing model. Fibrin gels containing 56 μg/mL aprotinin-α_2-PI$_{1-8}$ alone (CTRL) or with 2 μg/mL α_2-PI$_{1-8}$-VEGF$_{164}$ were placed on circular wounds in either nonischemic or ischemic dorsal skin flaps in Sprague–Dawley rats. (*A* and *B*) Tissues were harvested 7 d later, and paraffin sections were immunostained to detect endothelial cells [von Willebrand Factor (vWF)], pericytes (NG2), and smooth-muscle cells (SMA). $n = 6$. (Scale bar: 20 μm.) Arrowheads, α-SMA–positive microvessels and small-caliber arterioles and venules. (*C* and *E*) The amount of angiogenesis was quantified as vessel length density (VLD), and results are shown as mean ± SEM ($n = 5$–10 fields per group); ***$P < 0.001$, **$P < 0.002$. (*D* and *F*) Tissue blood perfusion was quantified by laser Doppler imaging after flap elevation with (*F*) or without (*D*) arterial ligation [postoperative (postop)] and 3 d and 7 d after gel implantation. Results show the amount of perfusion as a percentage of the nonischemic baseline set at 100% (mean ± SEM; $n = 6$); *$P < 0.05$. (*G*) Representative laser Doppler images of nonischemic and ischemic wounds (*Left* and *Right* side of each image, respectively) 7 d after treatment with control gels (CTRL) or α_2-PI$_{1-8}$-VEGF$_{164}$.

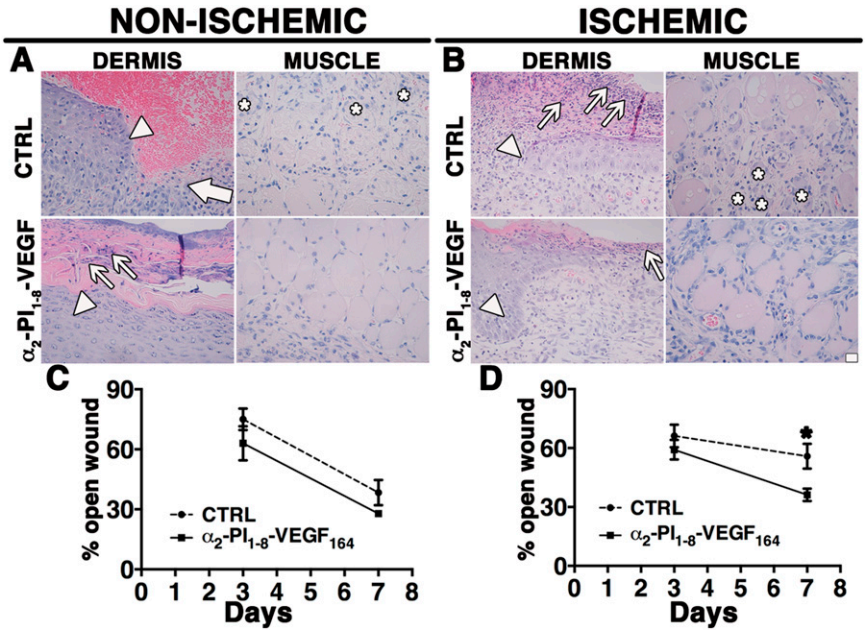

Fig. S9. α_2-PI_{1-8}-$VEGF_{164}$ significantly improves wound regeneration in an ischemic wound-healing model. Fibrin gels containing 56 μg/mL aprotinin-α_2-PI_{1-8} alone (CTRL) or with 2 μg/mL α_2-PI_{1-8}-$VEGF_{164}$ were placed on circular wounds in either nonischemic or ischemic dorsal skin flaps in Sprague–Dawley rats. (*A* and *B*) Tissues were harvested 7 d later, and paraffin sections were stained with H&E. Images were acquired both in the superficial layer (DERMIS) and in the underlying muscle layer (MUSCLE). $n = 6$. (Scale bar: 20 μm.) Arrowheads, epidermal hyperplasia; thick arrow, bleeding area; asterisks, monocyte infiltration of muscle fibers; thin arrows, keratinized tissue with apoptotic bodies. (*C* and *D*) Wound healing was measured by planimetric analysis 3 and 7 d after gel implantation, and results show the size of still-open wounds as a percentage of the initial size at day 0, set at 100% (mean ± SEM; $n = 6$); $^*P < 0.05$.